Energetic particle precipitation into the middle atmosphere triggered by a coronal mass ejection

Mark A. Clilverd[1], Craig J. Rodger[2], Robyn M. Millan[3], John G. Sample[4], Michael Kokorowski[5], Michael P. McCarthy[5], Thomas Ulich[6], Tero Raita[6,] Andrew J. Kavanagh[7], and Emma Spanswick[8].

Abstract. Precipitation of relativistic electrons into the atmosphere has been suggested as the primary loss mechanism for radiation belt electrons during large geomagnetic storms. Here, we investigate the geographical spread of precipitation as a result of the arrival of a coronal mass ejection (CME) on 21 January 2005. In contrast to previous statistical studies we provide one of the first attempts to describe the geographic and temporal variability of energetic particle precipitation on a global scale using an array of instruments. We combine data from subionospheric VLF radio wave receivers, the high altitude MINIS balloons, riometers, and pulsation magnetometers during the first hour of the event. There were three distinct types of energetic electron precipitation observed, one globally, one on the dayside, and one on the nightside. The most extensively observed form of precipitation was a large burst starting when the CME arrived at the Earth, where electrons from the outer radiation belt were lost to the atmosphere over a large region of the Earth. On the dayside of the Earth (10-15 MLT) the CME produced a further series of precipitation bursts, while on the nightside dusk sector (~20 MLT) a continuous precipitation event lasting ~50 minutes was observed at $2.5<L<3.7$ along with Pc 1-2 pulsations observed with a ground-based magnetometer. These observations suggest the generation of energetic electron precipitation at the inner edge of the outer radiation belt from EMIC wave scattering into the loss cone, and is the most direct evidence to date connecting EMIC activity and energetic precipitation.

1. Introduction

When a coronal mass ejection (CME) hits the Earth's magnetosphere the dayside magnetopause is compressed towards the Earth. At geostationary orbit increases or decreases in relativistic electron fluxes are observed [Reeves, 1998] depending on the severity of the shock associated with the CME, and a complex interplay between loss and acceleration processes [Horne and Thorne, 2003]. Energetic electrons are believed to be lost from geostationary orbit (and the outer radiation belt generally) by three possible mechanisms: (1) adiabatic motion; (2) magnetopause encounters; and (3) precipitation into the atmosphere [Lorentzen et al., 2001; Green et al., 2004; O'Brien et al., 2004; Selesnick et al., 2006]. Adiabatic motion caused by the stretching of magnetospheric field lines during a magnetic storm, known as the D_{st} effect, has been suggested as the primary cause of the flux decreases, but does not lead to a permanent loss of electrons. However, recent work by Ukhorskiy et al. [2006] has indicated that storm time intensification of the ring current produces an expansion of electron drift orbits such that their paths intersect the magnetopause leading to rapid electron loss. Precipitation into the atmosphere of electrons driven into the bounce loss cone has also been suggested as the primary loss mechanism, through interaction with electron cyclotron harmonic waves [Horne and Thorne, 2000], electromagnetic ion cyclotron waves [Summers and Thorne, 2003], or whistler waves [Horne and Thorne, 2003], either separately or in combination.

This paper describes the geographic and temporal variability of the loss of electrons to the atmosphere, as a result of the CME on 21 January 2005. Relativistic Electron Precipitation (REP) into the atmosphere has been observed to take several forms. Clilverd et al. [2006] showed that a series of bursts of precipitation into the middle atmosphere, each lasting several minutes, could be observed following the CME of 21 January 2005. Precipitation events lasting minutes to hours have previously been observed from the MAXIS balloon. They were observed between *L*=4-7, in the late afternoon/dusk sector, and may be produced by EMIC waves [Millan et al., 2002]. Loss rates suggest that these minute-hour events are a primary loss mechanism for outer zone relativistic electrons. During the 21 January 2005 CME event the total precipitation into the atmosphere could account for up to 50% of the >2 MeV electron flux losses in the outer radiation belt at the time [Clilverd et al., 2006].

When energetic electrons precipitate into the atmosphere they ionize the neutral atmosphere constituents, changing the existing electron density altitude profiles, driving chemical reactions, and generating bremsstrahlung X-rays from the collisions. The altitude at which the ionization occurs is dependent on the energy of the particle, with more energetic particles penetrating deeper into the atmosphere, e.g., 500 keV electrons produce peak ionization rates at ~70 km altitude. When a CME occurs in the presence of a solar proton event both precipitating electrons and protons can be present at the same time. Different instruments will observe the precipitation driven ionization increases in different ways.

Riometers (Little and Leinbach, 1959) will observe the integrated absorption of cosmic radio noise through the ionosphere, with increased absorption due to additional ionization due to both proton and electron precipitation. They have previously been shown to respond to the effects of CMEs [Brown et al., 1961; Osepian and Kirkwood, 2004]. The dominant altitude of the absorption is typically in the range 70-100 km i.e., biased towards relatively soft particle energies (>30 keV electrons), though significant solar proton precipitation (>10 MeV) will drive this altitude lower. Subionospheric VLF radio wave receivers that receive oblique incident radio waves are affected by the lowest altitude of significant ionization, thus the dominant altitude is set by the highest particle energies where there are significant high energy fluxes. If the electron precipitation energies are high enough to penetrate lower into the atmosphere than the proton precipitation, then variations in radio propagation conditions will be dominated by the electron precipitation. The opposite is true if the proton energies are dominant. Balloon-borne instruments detect bremsstrahlung radiation (20 keV–10 MeV) caused during energetic particle collision with the neutral atmosphere. The instruments are biased towards the highest energy precipitation present because the particles scatter at the lowest altitudes, and are relatively insensitive to low energy precipitation particularly when high energy precipitation is occurring.

In this study we analyze ground-based ionospheric data from mid and high latitudes during the arrival of a coronal mass ejection on 21 January 2005. We investigate the geographical spread of precipitation into the atmosphere as a result of the shock, and attempt to identify the processes that have driven it. We combine data from subionospheric VLF radio wave receivers, the high altitude MINIS balloons, riometers, and pulsation magnetometers to describe the geographic and temporal variability of energetic particle precipitation into the middle atmosphere during the first hour of the event. We particularly concentrate on describing the balloon and radio wave data because of their pre-disposition to monitor the impact of relativistic electron precipitation during this study period. We show that following the shock arrival there are significant differences in energetic particle precipitation between the dayside and the nightside driven by different wave-particle interactions, as well as significant differences in latitudinal structure.

2. Event conditions on January 21, 2005

An X7 solar flare at 06 UT on January 20, 2005 was followed in about 20 minutes by an unusually hard solar proton event. Recovery of the ionosphere due to the declining levels of proton flux was well underway late on 21 January when an associated coronal mass ejection (CME) triggered a K_p=8, D_{st}≈-100 nT geomagnetic storm, leading to a relativistic electron drop-out at geosynchronous orbit starting at ~17:10 UT. By 18 UT GOES-10 and GOES-12 >2 MeV electron fluxes had decreased by three orders of magnitude. The solar wind associated with the CME showed an increase from 600-900 km/s, and a density change from 6-16 protons cm^{-3} in less than 2 minutes (http://www.srl.caltech.edu/ACE/ASC/level2/swepam_l2desc.html). The shock was observed at ACE at 16:48 UT, and the propagation time to Earth was about 23 minutes, indicating an expected CME arrival time of 17:11 UT in our data.

In Figure 1 the changes in solar wind H^+ speed and density associated with the CME shock are shown. The data have been delayed by 23 minutes in order to represent the travel time from the ACE satellite to Earth. The lower panel shows the impact of the CME on the GOES relativistic electron fluxes measured at geostationary orbit.

3. Experimental setup

This paper combines data from subionospheric VLF radio wave receivers, the high altitude MINIS balloons, riometers, and pulsation magnetometers to describe the geographic and temporal variability of energetic particle precipitation into the middle atmosphere during the first hour of the event. This section describes the setup of each instrument, and relevance to this study. Clilverd et al. [2006] described observations showing energetic particle precipitation lasting 2.7 hours from the CME event, however, here we just concentrate on the initial period which shows the immediate effects of the shock arrival.

Here we use narrow band subionospheric VLF/LF data spanning 20-40 kHz received at three sites: Sodankylä, Finland (67ºN, 23ºE, *L*=5.2); Ny Ålesund, Svalbard (79ºN, 11ºE, *L*=18.3); and Halley, Antarctica (76ºS, 26ºW, *L*=4.7). These sites are part of the Antarctic-Arctic Radiation-belt Dynamic Deposition VLF Atmospheric Research Konsortia (AARDDVARK, see the description of the array at www.physics.otago.ac.nz/space/AARDDVARK_homepage.htm). The effects of changing ionization conditions in the mesosphere, due to energetic particle precipitation, can be observed along the propagation path between a transmitter and a receiver. Subionospheric propagation is sensitive to ionization located below about 90 km. The effect of increased ionization on the propagating signals can be seen as either an increase or decrease in signal amplitude or phase depending on the modal mixture of each signal observed [Barr et al., 2000].

The MINIS balloon project launched 6 balloons in January 2005 to observe the size, frequency and mechanisms of relativistic electron precipitation. The campaign staggered the launches in order to extend the longitudinal range over which relativistic electron precipitation could be observed. These balloons were launched from the South African Antarctic station, SANAE (72ºS, 2ºW) and Churchill, Canada (58.76ºN, 265.91ºE). The balloons carried Sodium Iodide (NaI) X-ray scintillation detectors used to detect Bremsstrahlung radiation (20 keV–10 MeV) caused during energetic particle collision with the neutral atmosphere, particularly those collisions at altitudes of 40-60 km. The MINIS balloon experiment observed significant X-ray counts from 17:10-17:40 UT on 21 January 2005. Most of the fluxes were observed from balloons at *L*=3.5 and *L*=4.1 in the southern hemisphere, although the first burst at 17:12 was also seen by a balloon at *L*=10 in the northern hemisphere [E. A. Bering III and the MINIS Team, *Multiple balloon observations of* *relativistic electron loss and associated electric and magnetic perturbations,* IAGA Scientific Assembly 2005, IAGA2005-A-00631].

The riometers used in this study are located either in the NORSTAR and MIRACLE arrays in Canada and Scandinavia respectively, or at Halley, Antarctica (76°S, 26°W, and L=4.5). The data from Kilpisjärvi, Finland, (69.02ºN, 20.86ºE) are taken from the central beam of the Imaging Riometer for Ionospheric Studies (IRIS) (Browne et al., 1995), which operates at 38.2 MHz. The Canadian riometers are widebeam, 30 MHz, vertical pointing parallel dipole systems, with time resolutions of 1-10 seconds, although we typically present 1 minute average data. The riometer data presented from Pinawa (50.20ºN, 263.96ºE, and L=4.1) in the NORSTAR array is on the dayside during the CME. Similarly Rankin is also in the NORSTAR array, on the dayside during the CME, and located at 62.82ºN, 267.87ºE, L=12.44 The IRIS riometer in Kilpisjärvi, Finland, was in the dusk sector during the CME, located at 69.02ºN, 20.86ºE, and at L=6.1. We also use Jyväskylä in Finland, which was also in the dusk sector, at 64.42ºN, 25.28ºE, and L=3.7 and operates at 32.4 MHz.

A latitudinal chain of pulsation magnetometers is located in Finland, and operated by the Sodankylä Geophysical Observatory. The magnetometers range from L=3.4-6.1, and operate with a time resolution of 0.025 s. We are principally interested in the Nurmijärvi site, located at 60.51ºN, 24.65ºE, and at L=3.4. Here we study the frequency range of 0.1-4 Hz. In this frequency range waves of ~2 Hz are thought to be generated by the electromagnetic ion cyclotron (EMIC) instability near the magnetic equator. Pc 1-2 waves propagate along the field line, and can also be observed on the ground [Erlandson et al., 1996]. Solar wind compressions of the magnetosphere can generate Pc 1 pulsations, as the compressions increase the ion anisotropy which, in turn, increases the EMIC wave growth rate [Kangas et al., 1986]. As previously mentioned, precipitation into the atmosphere of electrons driven into the bounce loss cone has been suggested as the primary loss mechanism from the radiation belts through interaction with EMIC waves [Summers and Thorne, 2003], although conclusive experimental evidence showing precipitation occurring during EMIC activity has yet to be reported. Arnoldy et al. [1982] found that pulsating aurora was accompanied by Pc1 ULF waves at Siple station, Antarctica (L=4.2) and closely associated with riometer absorption, all potentially linked through enhanced particle precipitation. Arnoldy et al. [1983] further observed that auroral light bursts were correlated with Pc1 wave packets recorded at Siple and suggested a mechanism of the acceleration and precipitation of electrons with auroral energies (few keV) by EMIC waves.

Figure 2 shows the location of the radio wave receiver sites (diamonds), and the transmitter-receiver paths that were under study during the event period (transmitter locations are given by the circles). The majority of the paths studied here are in the same longitude sector as the GOES-12 satellite. The solid squares show the location where the MINIS balloons were operating and hollow squares their equivalent conjugate based on the IGRF magnetic field model. Riometer sites which provided data for this study are shown by triangles, and the pulsation magnetometer site by a star. The location of the sunrise/sunset terminator are also shown (dotted line), America and Antarctica are daylit during the events. The CME occurred during the northern hemisphere winter, with North America being close to midday, and Europe being in the evening/dusk sector. The observations made in Antarctica in the southern hemisphere were fully sunlit, and close to midday as well. Additional data from an Australian site is included later in the study. Australia was close to midnight at the time of the CME.

4. Results

(i) Dayside observations (10-15 MLT)

In this section we describe the dayside precipitation characteristics during the CME. Figure 3 shows northern hemisphere riometer data from Rankin (*L*=12.4), Pinawa (*L*=4.1), and radio wave data from North Dakota (NDK, 25.2 kHz) received at Sodankylä Geophysical Observatory (SGO), Finland, where the transmitter-receiver great circle path stretches from *L*=3-15. The time axis covers the first hour of the CME event. The solid vertical dashed line shows the start of the CME-arrival associated precipitation in all three panels. The precipitation at onset is seen at both riometers at *L*≈12 and *L*≈4 (17:12 UT, ~10:30 MLT), and also occurs on the MINIS balloon at *L*=10 (17:12 UT, ~ 12:30 MLT, not shown). Both Rankin and the *L*=10 balloon do not observe any significant variations following the initial pulse which is consistent with their high latitude locations, and field-line positioning outside the dayside magnetosphere (e.g., open field lines). Note that the consistently higher absorption at Rankin *(L*=12.4) is a consequence of the solar proton precipitation resulting in polar cap absorption (e.g. Reid, 1974). Pinawa (*L*=4.1) is sufficiently equatorward to be inaccessible to the bulk of the solar proton flux because of the influence of geomagnetic rigidity cutoffs [Rodger et al., 2006].

In Figure 3 three additional vertical dashed lines have been added to identify periods where bursts of precipitation have occurred. The bursts are seen on the Pinawa riometer (*L*=4.1) and the radio wave data from the nearby North Dakota transmitter, and are ~14 minutes apart, lasting about 50 minutes in all. The signatures in the radio wave data suggest that some of the electron precipitation is at high energies (>400 keV) in order for them to dominate over the ongoing solar proton precipitation event, and the normal daytime solar photo-ionization levels. Each burst of precipitation appears to last longer, extending from the initial ~6 minutes, to ~15 minutes by the fourth burst. This is consistent with the idea that lower energy electrons are taking longer each time to come into the field of view. A comparison between the reducing levels of radio wave amplitude effects and the increasing riometer absorption levels for each successive burst suggests that the precipitation disperses in time, and softens in energy spectra. Figure 1 indicates that there is no clear signature of a periodic driver in the solar wind that could be causing periodicity in the precipitation bursts.

Measurements made during the CME on the southern hemisphere dayside are shown in Figure 4. The data span a range of 3.5<*L*<5. A solid vertical line, and three vertical dashed lines have been added to identify the times when bursts of precipitation were observed in the northern hemisphere data. The MINIS balloon measurements during the study period were made north-east of Halley, Antarctica (76°N, 26°W, ~15 MLT), while the radio wave data was taken from the Hawaii transmitter (NPM, 21.4 kHz) to the west of Halley (~12 MLT). The region of sensitivity of the Hawaii-Halley path is shown as a heavy line on the path in Figure 2, and results from increased propagation sensitivity to boundary conditions over the thick ice shelf of Antarctica (Clilverd et al., 2005).

Widebeam riometer data from Halley is also shown in Figure 4, representing precipitation at *L*=4.5. The shock onset and first additional precipitation burst are reasonably timed with respect to the bursts observed in the northern hemisphere, although there is clearly additional precipitation being detected in the region around Halley. The MINIS balloon data contains some data gaps due to the loss of the Iridium satellite connection, but the *L*=4.1 balloon shows event occurrence that is consistent with the northern hemisphere timing. The *L*=3.5 balloon is largely unaffected and may therefore represent a lower *L*-shell limit for this behavior. The Balloon MLT (15-16 MLT) during this event is approximately the same as that given for Halley although they are located slightly east of the station at the time (see Figure 1).

The radio wave data shown in the upper panel similarly identifies the initial burst of energetic precipitation at the same time as all of the instruments, but thereafter only indicates that some precipitation is occurring in the region west of Halley. This is primarily because of the combination of local precipitation overlapping with the large scale bursts of precipitation, and the smearing effect of the Hawaii to Halley path looking over a large range of longitudes. Overall the southern hemisphere dayside data also shows burst activity lasting about 50 minutes caused by energetic electron precipitation, and the timing characteristics are the same as those in the northern hemisphere.

In order to compare the riometer and balloon data more closely we analyze a shorter period in detail. Figure 5 shows the period between 17:18-17:45 UT. Four significant peaks in L=4.5 riometer absorption can be seen in the period, identified on the plot as '1', '2', '3', and '4'. Each of the peaks are captured in the balloon data, although peak '4' is missing in the L=4.1 balloon because of a data gap. Peaks '2' and '3' are seen in the L=4.1 balloon data, but only as a sharp increase in x-ray count rate at the very beginning of the event. The duration of each event is typically 1 minute in the balloon data in contrast to 4 minutes in the riometer data. The balloon-bourne experiment observes the production of bremsstrahlung ionization continuously overhead for ~1 minute. Any low altitude recombination of the ionization is extremely fast at low altitudes, and the end of the event is most likely to be associated with the end of the precipitation. The riometer responds to the production and decay of the additional ionization from higher altitudes during the precipitation event. Peak '4' is seen as a short-lived event by the riometer and the L=3.5 balloon, and is spread over a larger range of L-shells than events '2' and '3'. Further work is planned on the response of these two instruments during the 3 last peaks identified here.

(ii) Duskside observations (~20 MLT)

In this section we describe the duskside precipitation characteristics during the CME. Figure 6 shows northern hemisphere riometer data from Kilpisjärvi (L=6.1), Jyväskylä (L=3.7), both in Finland, and radio wave data from Iceland (NRK, 37.5 kHz) and Germany (DHO, 23.4 kHz) both received at SGO, Finland (L=5-6, and L=2.5-5 for the span of the paths respectively). Again, the time axis covers the first hour of the CME event. The solid vertical line shows the start of CME precipitation in all four panels (17:12 UT, ~20 MLT).

At about L~6 the riometer and the radio wave data are very consistent. They both show the initial burst of energetic precipitation at the start of the CME event, but within 10-15 minutes there are no signs of any further disturbances. The elevated background absorption levels on the Kilpisjärvi riometer are consistent with a quasi-constant background of ionization from the solar proton event. These observations are interpreted as indicating that a burst of precipitation occurred as the magnetosphere was compressed to L~6, but afterwards that there was no significant influence of the solar wind dynamics, primarily because of the region being on the duskside of the Earth.

At L~4, shown by Jyväskylä at L=3.7, the picture appears quite similar with a burst of enhanced ionization at the start of the CME, followed by a relatively flat response until a small absorption event at about 18:10 UT. However the DHO-SGO radio wave data from the propagation path that spans $2.5<L<5.2$ (Germany to Finland) there is a clear signature of energetic precipitation occurring from the onset of the CME arrival, and lasting about 50 minutes. On the plot the near-horizontal dashed line has been added to provide a representation of the likely non-disturbed amplitude levels using quiet-time data from before and after the storm period. In Figure 7 we contrast the phase and amplitude data from the DHO-SGO path with data taken from the NLK-Ny Ålesund path (Seattle to Svalbard) recorded during the X45 solar flare on 4 November 2003, also known as Thomson's Great Flare (Thomson et al., 2005).

As before, near-horizontal lines have been added to the panels to indicate the likely phases and amplitudes that would have occurred if the enhanced ionization had not been present. The similarity between the two events is striking, and clearly show that in the same way as a very large solar flare, the CME event lead to sustained period of enhanced ionization on the nightside and not the bursts of precipitation-induced ionization which we observe on the dayside. The phase and amplitude data show us that the peak in precipitation flux on the DHO-SGO path was at 17:21 UT, and the event lasted from 17:12-17:57 UT. The lack of this signature in the Jyvaskyla riometer data suggests the possibility that the energetic precipitation is only occurring for $2.5<L<3.7$.

An energetic precipitation event lasting ~45 minutes is consistent with the length of precipitation events reported by the MAXIS balloon experiment [Millan et al., 2002], although the *L*-shell range in this event is lower than the range of $4<L<7$ that MAXIS was primarily observing. Millan et al. [2002] proposed EMIC waves as the possible precipitation driver, due to the balloon-observed *L*-shell range and local time dependence of the precipitation events observed. In Figure 8 we show the pulsation magnetometer data from Nurmijärvi, Finland, located at 60.51ºN, 24.65ºE, $L=3.4$. Strong Pc-1 waves in the frequency range 0.5-2.5 Hz were detected following the CME, lasting until 18:06 UT. The EMIC wave power began in the frequency range 0.5-1.0 Hz from 17:14-17:32 UT, followed by a sudden change to 2.0-2.5 Hz which lasted for the remainder of the event (~30 minutes more). At the top of the plot we show the mean EMIC wave power in the band 0.5-3 Hz. The noise floor prior to the arrival of the CME is defined at the 0 dB level. The peak EMIC wave power is observed at 17:20 (17.33) UT which is consistent with the timing of the maximum electron precipitation effect observed on the DHO-SGO path, i.e., Figure 7.

The EMIC was measured simultaneously at every station in the latitudinal array in Finland. The highest power was seen at the southern most station (Nurmijärvi) indicating that the EMIC wave was generated on a low latitude field line, either near L=3.4 or lower and that the wave propagated long distances in the ionosphere. The polarization of the wave was predominantly left handed, again confirming the EMIC source. The duration and latitude of the EMIC is entirely consistent with the continuous precipitation observed in the DHO-SGO radio wave data, and the EMIC waves are therefore a strong candidate as the cause of the precipitation observed.

(iii) Nightside observations (~04:30 MLT)

In this section we briefly describe the nightside precipitation characteristics during the CME. Figure 9 shows southern hemisphere riometer data from Macquarie Island (54.50ºS, 158.95ºE, and L=5.4), south of Australia. The CME arrived at the Earth at ~04:30 MLT at this longitude. A clear signature of the initial burst of precipitation can be seen at 17:12 UT confirming that this feature is observed all of the way around the Earth. Additional precipitation at this longitude occurs following the CME, but does not have any of the same temporal characteristics of the dayside riometer data. With no co-incident radio wave or MINIS balloon data in this longitude sector at this time it is difficult to describe the spectral makeup of the precipitation.

Radio wave data recorded between New Zealand and Australia at this time, simply indicates that there was no signature of precipitation during this event for L<2.7 (N. R. Thomson – personal communication). Which is consistent with the L-shell range, 3<L<12, already suggested for the initial burst of precipitation.

7. Discussion and Summary

Energetic particle precipitation into the middle atmosphere occurred in three different ways as a result of the CME at 17:12 UT on 21 January 2005. In Figure 10 we summarize the regions affected by precipitation during the first hour following the arrival of the CME. The likely precipitation mechanisms are indicated in the key. The most commonly observed form of precipitation was a burst at the onset of the CME arrival lasting about 5-8 minutes. This was observed by all the instruments involved in this study, and covered a large range of L-shells (at least $3<L<12$), as well as daytime and nighttime longitudes. Thus electrons from the outer radiation belt were lost to the atmosphere over a large region of the Earth following the arrival of the CME shock. The burst of energetic electron precipitation was energetic enough to generate significant additional ionization at lower altitudes than the ongoing solar proton precipitation event, and also lower than the altitude of the daytime lower ionosphere on the dayside at ~72 km. This typically requires electron energies of >400 keV. The mechanism driving the precipitation is likely to be due to the sudden compression of the magnetospheric field lines when the solar wind pressure increased. The initial pulse of energetic electron precipitation clearly affected a wide part of the Earth's atmosphere. On the basis of our experimental measurements, the minimum extent that roughly spanned L= 3 to 12, both hemispheres, and all longitudes (360º in extent), translates to ~15% of the Earth's atmosphere at 100 km.

On the dayside of the Earth (10-15 MLT) the CME produced a series of precipitation bursts, following the initial burst. The time delay between each successive precipitation burst was approximately the same (~14 minutes). The bursts are observed to last for ~50 minutes after the CME arrival onset, and then die away. The times of the end of each burst of precipitation appears to be increasingly delayed with respect to the start, and they suggest a period of ~17 minutes. The longer duration of enhanced absorption with each successive burst is also consistent with the energy dispersion that would occur in a recurring population of drifting electrons.

These observations are consistent with the idea that the precipitation is being caused by a recurring body of particles that are in a drift orbit around the Earth at

L~4. Using expressions from Walt [1994] we find that the azimuthal drift period around the Earth at L=4.0 for 1.5 MeV electrons with a pitch angle of 90 degrees, i.e., equatorially trapped, is ~14 minutes, while for electrons of 800 keV energy this is 17 min. For marginally trapped electrons the 14 minute drift period would equate to electrons energies of ~1 MeV.

Interestingly, the repetitive burst precipitation is not observed on the duskside, suggesting that although the energetic electrons are orbiting the Earth, the precipitation mechanism is mainly located on the dayside. The most likely mechanisms for this are scattering into the loss cone by VLF chorus waves, or electron cyclotron harmonic (ECH) waves. ECH waves are typically found on the dayside only, and close to the magnetopause [Kennel et al., 1970; Anderson and Maeda, 1977] thus they fit the picture of a dayside mechanism. ECH waves, though, are not able to produce electron precipitation with energies of ~1 MeV, as they resonate with electrons of only a few keV [Horne et al., 2003]. However, the broadband VLF receiver at Halley was detecting VLF chorus (0.5-2 kHz) on the dayside at the start of the CME. The wave signatures disappeared at 17:12 UT probably as a result of increased ionospheric absorption of the chorus, rather than the chorus stopping itself. Chorus, especially the lower frequency components, that occur away from the geomagnetic equator can interact with, and precipitate, MeV electrons [Lorentzen et al., 2001].

On the nightside dusk sector (~20 MLT) there is little energetic particle precipitation for L>3.7 once the CME arrival onset burst has occurred. However, at lower L-shells 2.5<L<3.7 a precipitation event lasting ~50 minutes is observed. The precipitation is not bursty, but continuous, peaking at 17:35 UT, i.e. ~9 minutes after the CME onset. At the same time a Pc-1 EMIC wave was detected at L=3.4 in the pre-midnight dusk sector. The EMIC wave was observed at 0.5-2.5 Hz, from 17:12-18:06 UT. EMIC waves are normally observed near the plasmapause, and with K_P~8 at this time the plasmapause would be expected to be forced inwards towards L=2-3. These observations are consistent with the generation of energetic electron precipitation at the inner edge of the outer radiation belt from EMIC wave scattering into the loss cone, and is the most direct link between EMIC activity and energetic precipitation observed thus far.

Acknowledgments. The authors would like to thank Frank Skogen of the Kings Bay Company for overseeing the collection and return of the Ny Ålesund data. We would also like to thank the Australian World Data Center for the Macquarie Island data. The MINIS campaign was funded by the National Science Foundation of Polar Programs and Atmospheric Sciences Division. The Kilpisjärvi riometer data is from the wide beam of the Imaging Riometer for Ionospheric Studies (IRIS), operated by the Department of Communications Systems at Lancaster University (UK) in collaboration with the Sodankylä Geophysical Observatory, and is funded by the Particle Physics and Astronomy Research Council (PPARC).

References

Anderson, R. R., and K. Maeda (1977), VLF emissions associated with enhanced magnetospheric electrons, J. Geophys. Res., 82, 135-146.

Arnoldy, R. L., K. Dragoon, L. J. Cahill, S. B. Mende, and T. J. Rosenberg (1982), Detailed correlations of magnetic-field and riometer observations at L=4.2 with pulsating aurora, J. Geophys. Res., 87, 10449-10456.

Arnoldy, R. L., R. L. Kaufmann, L. J. Cahill, and S. B. M. Lockheed (1983), Pc1 pearl–electron interactions on the L=4.2 magnetic shell, Geophys. Res. Lett., 10, 627-630.

Barr, R., D. L. Jones, and C. J. Rodger (2000), ELF and VLF radio waves, J. Atmos. Sol.-Terr. Phys., 62, 1689-1718.

Brown, R. R., T. R. Hartz, B, Landmark, H. Leinbach, and J. Ortner, (1961), Large-Scale Electron Bombardment of the Atmosphere at the Sudden Commencement of a Geomagnetic Storm, J. Geophys. Res., 66, 1035–1041.

Browne, S., J. K. Hargreaves, and B Honary, (1995): An Imaging Riometer for Ionospheric Studies, Elect. Comm. Eng. J., 7, 209–217.

Clilverd, M. A., C. J. Rodger, Th. Ulich, A. Seppälä, E. Turunen, A. Botman, and N. R. Thomson (2005), Modelling a large solar proton event in the southern polar cap, J. Geophys. Res., 110(A9), doi: 10.1029/2004JA010922.

Clilverd, M. A., C. J. Rodger, and Th. Ulich (2006), The importance of atmospheric precipitation in storm-time relativistic electron flux drop outs, Geophys. Res. Lett., Vol. 33, No. 1, L01102, doi:10.1029/2005GL024661.

Erlandson, R. E., K. Mursula, and T. Bosinger (1996), Simultaneous ground-satellite observations of structured Pc-1 pulsations, J. Geophys. Res., 101, 27149-27156.

Green, J. C., T. G. Onsager, T. P. O'Brien, and D. N. Baker (2004), Testing loss mechanisms capable of rapidly depleting relativistic electron flux in the Earth's outer radiation belt, J. Geophys. Res., 109, A12211, doi:10.1029/2004JA010579.

Horne, R. B., and R. M. Thorne, (2000), Electron pitch angle diffusion by electrostatic electron cyclotron harmonic waves: the origin of pancake distributions, J. Geophys. Res. Vol. 105, No. A3, p. 5391 (1999JA900447).

Horne, R. B., and R. M. Thorne, (2003), Relativistic electron acceleration and precipitation during resonant interactions with whistler-mode chorus, Geophys. Res. Lett., 30(10), 1527, doi:10.1029/2003GL016973.

Horne, R. B., R. M. Thorne, N. P. Meredith, and R. R. Anderson (2003), Diffuse auroral electron scattering by electron cyclotron harmonic and whistler mode waves during an isolated substorm, J. Geophys. Res. Vol. 108, No. A7, 1290, doi:10.1029/2002JA009736.

Kangas, J., A. Aikio, and J. V. Olson (1986), Multistation correlation of ULF pulsation spectra associated with sudden impulses, Planet. Space Sci., 34, 543-553.

Kennel, C. F., F. L. Scraf, R. W. Fredrick, J. H. McGehee, and F. V. Coroniti (1970), VLF electric field observations in magnetosphere , J. Geophys. Res., 75, 6136-6152.

Little, C.G. and H. Leinbach, (1959), The riometer: a device for the continuous measurements of ionospheric absorption, Proc. IRE, 37, 315-320.

Lorentzen, K. R., J. B. Blake, U. S. Inan, J. Bortnik (2001), Observations of relativistic electron microbursts in association with VLF chorus, J. Geophys. Res. Vol. 106 (A4): 6017-6027.

Millan, R. M., R. P. Lin, D. M. Smith, K. R. Lorentzen, and M. P. McCarthy (2002), X-ray observations of MeV electron precipitation with a balloon-borne germanium spectrometer, Geophys. Res. Lett., 29(24), 2194, doi:10.1029/2002GL015922.

O’Brien, T. P., M. D. Looper, and J. B. Blake (2004), Quantification of relativistic microburst losses during the GEM storms, Geophys. Res. Lett., 31, L04802, doi:10.1029/2003GL019153.

Osepian, A., and S. Kirkwood (2004), Cosmic radio-noise absorption bursts caused by solar wind shocks, Ann. Geophys., 22, 2973-2987.

Reeves, G. D. (1998), Relativistic electrons and magnetic storms: 1992-1995**,** Geophys. Res. Lett., 25(11), p. 1817 (98GL01398).

Rodger, C. J., M. A. Clilverd, P. T. Verronen, Th. Ulich, M. J. Jarvis, and E. Turunen, Dynamic geomagnetic rigidity cutoff variations during a solar proton event, J. Geophys. Res., 111, A04222, doi:10.1029/2005JA011395, 2006.

Selesnick, R. S. (2006), Source and loss rates of radiation belt electrons during magnetic storms, J. Geophys. Res., 111(A4), A04210, doi:10.1029/2005JA011473.

Summers, D., and R. M. Thorne (2003), Relativistic electron pitch-angle scattering by electromagnetic ion cyclotron waves during geomagnetic storms, J. Geophys. Res., 108(A4), 1143, doi:10.1029/2002JA009489.

Thomson, N. R., C. J. Rodger, and M. A. Clilverd (2005), Large solar flares and their ionospheric D region enhancements, J. Geophys. Res., Vol. 110, No. A6, A06306, doi:10.1029/2005JA011008.

Ukhorskiy A. Y., B. J. Anderson, P. C. Brandt, and N. A. Tsyganenko (2006), Storm time evolution of the outer radiation belt: Transport and losses, J. Geophys. Res., Vol. 111, No. A11, A11S03, doi:10.1029/2006JA011690.

Walt, M. (1994), Introduction to Geomagnetically Trapped Radiation, Cambridge Atmospheric and Space Series, Cambridge Univ. Press, pp 49.

---

[1]M. A. Clilverd, Physical Sciences Division, British Antarctic Survey, High Cross, Madingley Road, Cambridge CB3 0ET, England, U.K. (email: macl@bas.ac.uk)

[2]C. J. Rodger, Department of Physics, University of Otago, P.O. Box 56, Dunedin, New Zealand. (email: crodger@physics.otago.ac.nz)

[3]R. M. Millan, Dartmouth College, Dept., of Physics and Astronomy, 127 Wilder Lab., Hanover, NH 03755 (email: robyn.millan@dartmouth.edu)

[4]J. G. Sample, Physics Dept., University of California, Space Sciences Lab., Berkeley, CA 94720-7450. (email: jsample@ssl.berkeley.edu)

[5]M. Kokorowski and M. P. McCarthy, Dept., of Earth and Space Science, University of Washington, 266 Johnson Hall 351310, Seattle, WA 98195. (email: mkoko@washington.edu and mccarthy@ess.washington.edu)

[6]Th. Ulich and T. Raita, Sodankylä Geophysical Observatory, University of Oulu, Sodankylä, Finland. (email: Thu@sgo.fi and tero.raita@sgo.fi)

[7]A. J. Kavanagh, Space Plasma Environment and Radio Science group, Dept., Communication Systems, InfoLab 21, Lancaster University, Lancaster, LA1 4WA, UK. (email: a.j.kavanagh@lancaster.ac.uk)

[8]E. Spanswick, Dept. of Physics and Astronomy, University of Calgary, 2500 University Drive, Calgary, Alberta, Canada T2N 1N4 (email: emma@phys.ucalgary.ca)

(Received N x, 2007; N x 27, 2007;

accepted N x, 2007.)

Figure 1. Solar wind parameters, and GOES-12 electron fluxes during the CME on 21 January 2005, showing the conditions expected at the Earth based on delayed ACE measurements.

Figure 2. (Left**)** The location of subionospheric propagation paths in the northern hemisphere from VLF transmitters to the AARDDVARK receiver sites at Ny Ålesund, and Sodankylä. The locations of MINIS balloons are indicated by squares, riometer locations by triangles and pulsation magnetometer by a star. The day/night terminator is also shown by a dotted line. (Right) The equivalent map for the southern hemisphere, with the propagation paths from the Hawaii VLF transmitter to Halley, Antarctica is shown, as well as the Halley riometer.

Figure 3. The dayside northern hemisphere data from the Rankin and Pinawa riometers, and the radio wave data from North Dakota for 17:00-18:18 UT on 21 January 2005. The start of energetic particle precipitation bursts are identified by vertical dashed lines. The *L*-shells that the observations were made at are indicated on the plot.

Figure 4. The dayside southern hemisphere data recorded in Antarctica from 17:00-18:18 UT on 21 January 2005. Radio wave data from Hawaii, recorded at Halley, and data from two MINIS balloons are shown. The start of energetic particle precipitation bursts are identified by vertical dashed lines. The *L*-shells that the observations were made at are indicated on the plot.

Figure 5. The dayside southern hemisphere data recorded in Antarctica from 17:18-17:45 UT on 21 January 2005. Comparisons are shown of data from the two MINIS balloons, and the Halley riometer.

Figure 6. The nightside northern hemisphere data from 17:00-18:18 UT on 21 January 2005. Radio wave data from Iceland and Germany, recorded at Sodankylä, Finland, and data from two Finnish riometers are shown. The *L*-shells that the observations were made at are indicated on the plot.

Figure 7. The phase and amplitude of radio wave transmissions from Germany (DHO) received at Sodankylä, Finland following the CME onset at 17:12 UT on 21 January 2005. The right-hand panels contrast the data from Seattle (NLK) received at Ny Ålesund, Svalbard, during Thomson's Great Flare of 4 November 2003, indicating a continuous source of ionization following the CME in January 2005.

Figure 8. The Nurmijärvi (L=3.4) pulsation magnetometer data from 17:00-18:18 UT on 21 January 2005 showing the presence of Pc1 pulsations following the CME. The top panel shows the mean power in the range 0.5-3 Hz in dB above the noise floor.

Figure 9. The nighttime Macquarie riometer data showing the initial burst of precipitation following the CME at 17:12 UT on 21 January 2005 (03:30 MLT).

Figure 10. A summary map showing the regions affected by bursts of precipitation triggered by the arrival of the CME at 17:12 UT on 21 January 2005.

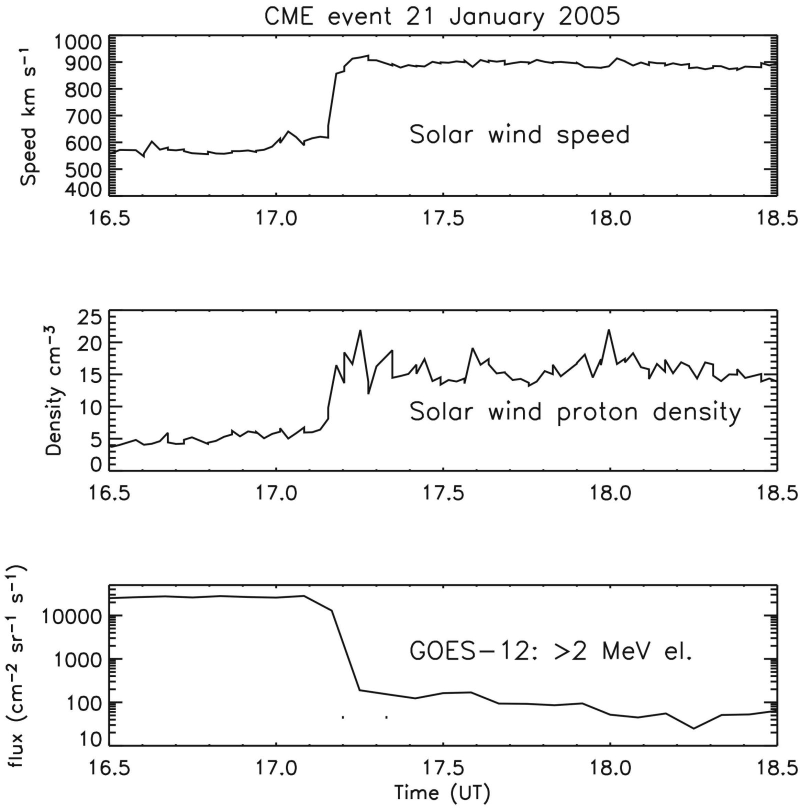

CME event 21 January 2005
Speed km s^{-1}
1000
900
800
700
600
500
400
Solar wind speed
16.5
17.0
17.5
18.0
18.5
Density cm^{-3}
25
20
15
10
5
0
Solar wind proton density
16.5
17.0
17.5
18.0
18.5
flux (cm^{-2} sr^{-1} s^{-1})
10000
1000
100
10
GOES−12: >2 MeV el.
16.5
17.0
17.5
18.0
18.5
Time (UT)

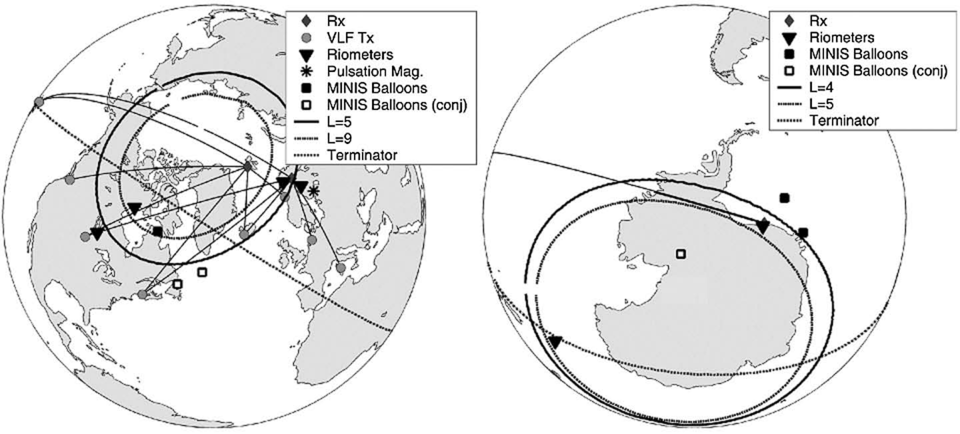

Rx
VLF Tx
Riometers
Pulsation Mag.
MINIS Balloons
MINIS Balloons (conj)
L=5
L=9
Terminator
Rx
Riometers
MINIS Balloons
MINIS Balloons (conj)
L=4
L=5
Terminator

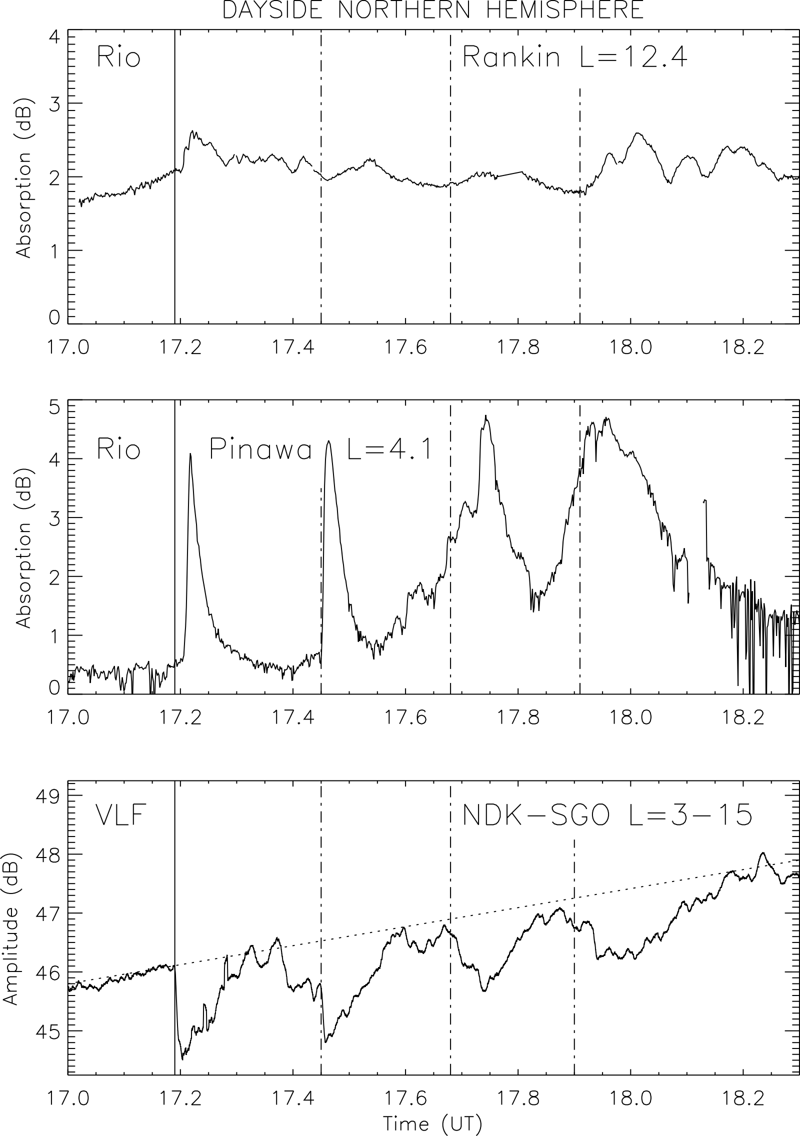

DAYSIDE NORTHERN HEMISPHERE
Rio
Rankin L=12.4
Absorption (dB)
0
1
2
3
4
17.0
17.2
17.4
17.6
17.8
18.0
18.2
Rio
Pinawa L=4.1
Absorption (dB)
0
1
2
3
4
5
17.0
17.2
17.4
17.6
17.8
18.0
18.2
VLF
NDK-SGO L=3-15
Amplitude (dB)
45
46
47
48
49
17.0
17.2
17.4
17.6
17.8
18.0
18.2
Time (UT)

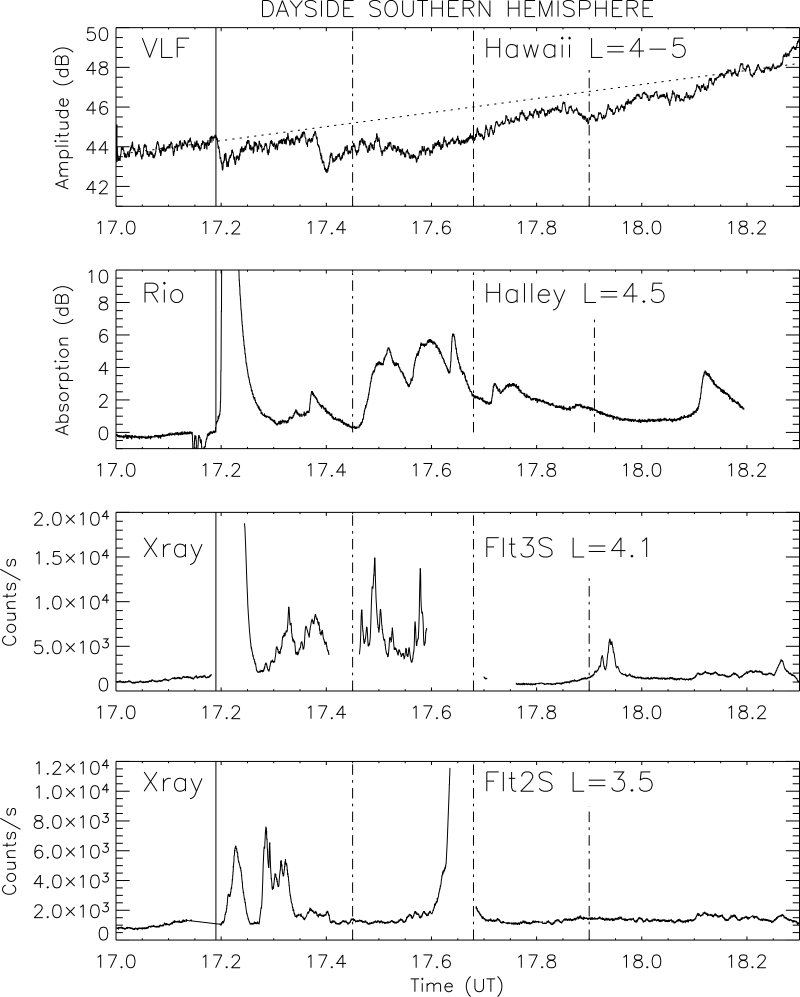
DAYSIDE SOUTHERN HEMISPHERE
VLF
Hawaii L=4−5
Amplitude (dB)
50
48
46
44
42
17.0
17.2
17.4
17.6
17.8
18.0
18.2
Rio
Halley L=4.5
Absorption (dB)
10
8
6
4
2
0
Xray
Flt3S L=4.1
Counts/s
2.0×10^4
1.5×10^4
1.0×10^4
5.0×10^3
0
Xray
Flt2S L=3.5
Counts/s
1.2×10^4
1.0×10^4
8.0×10^3
6.0×10^3
4.0×10^3
2.0×10^3
0
Time (UT)

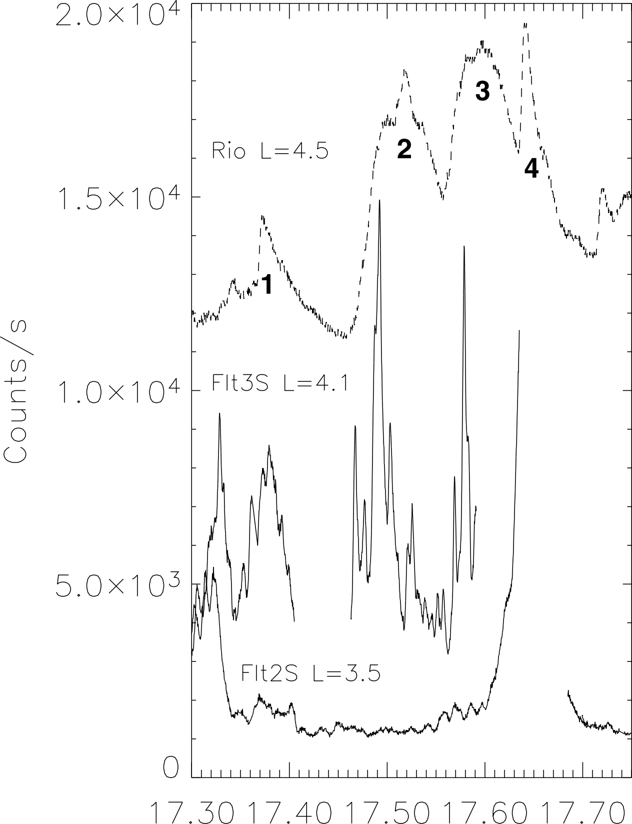

2.0×10^4
1.5×10^4
1.0×10^4
5.0×10^3
0
Counts/s
Rio L=4.5
Flt3S L=4.1
Flt2S L=3.5
1
2
3
4
17.30 17.40 17.50 17.60 17.70

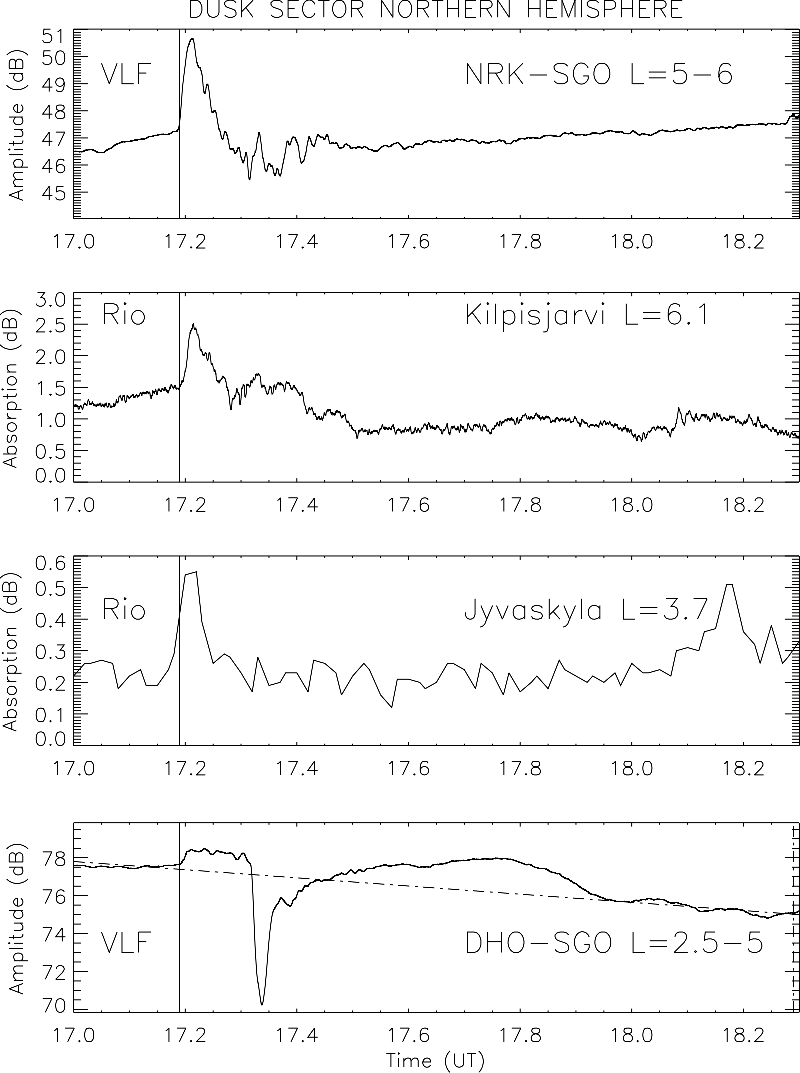
DUSK SECTOR NORTHERN HEMISPHERE
VLF
NRK−SGO L=5−6
Amplitude (dB)
Rio
Kilpisjarvi L=6.1
Absorption (dB)
Rio
Jyvaskyla L=3.7
Absorption (dB)
VLF
DHO−SGO L=2.5−5
Amplitude (dB)
Time (UT)

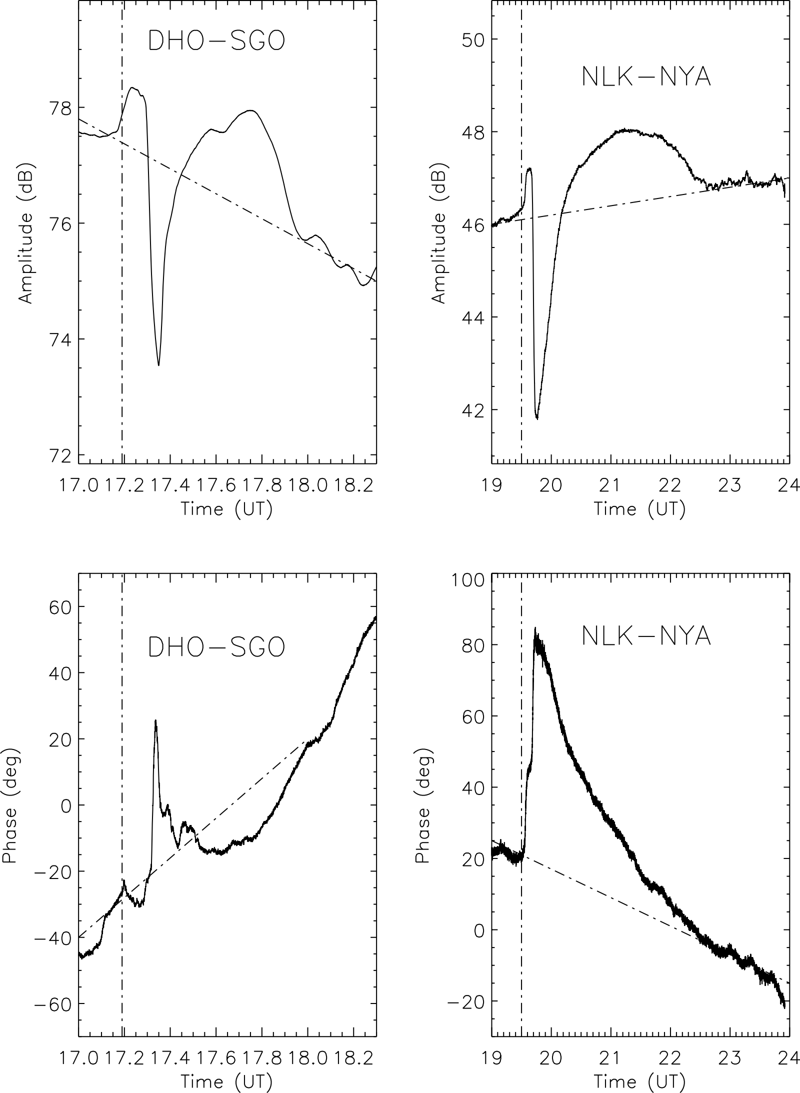

DHO−SGO
NLK−NYA
DHO−SGO
NLK−NYA
Amplitude (dB)
Phase (deg)
Time (UT)
78
76
74
72
50
48
46
44
42
60
40
20
0
−20
−40
−60
100
80
17.0
17.2
17.4
17.6
17.8
18.0
18.2
19
20
21
22
23
24

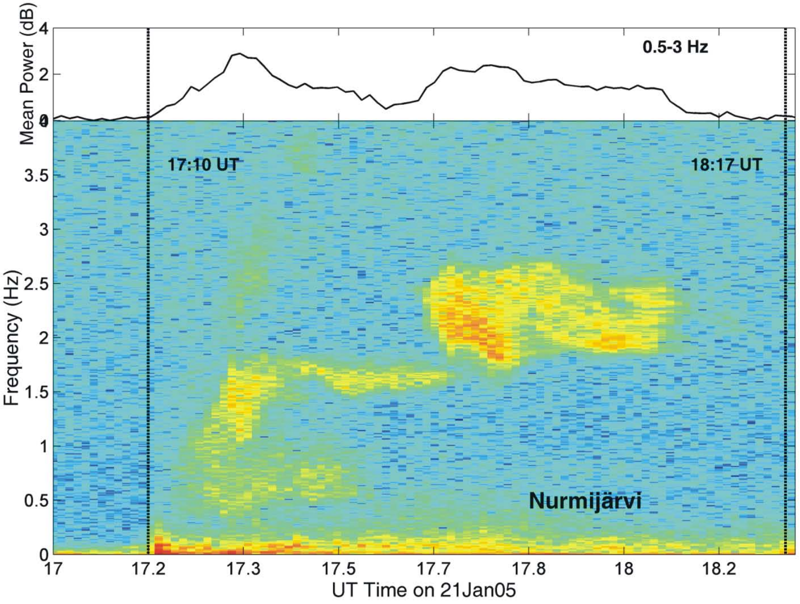

Mean Power (dB)
4
2
0
0.5-3 Hz
17:10 UT
18:17 UT
Frequency (Hz)
3.5
3
2.5
2
1.5
1
0.5
0
Nurmijärvi
17
17.2
17.3
17.5
17.7
17.8
18
18.2
UT Time on 21Jan05

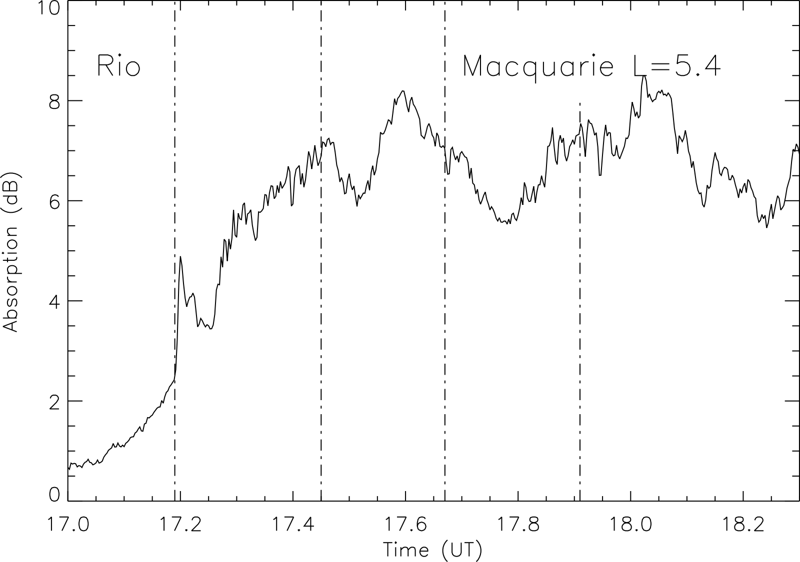
Rio
Macquarie L=5.4
Absorption (dB)
Time (UT)
0
2
4
6
8
10
17.0
17.2
17.4
17.6
17.8
18.0
18.2

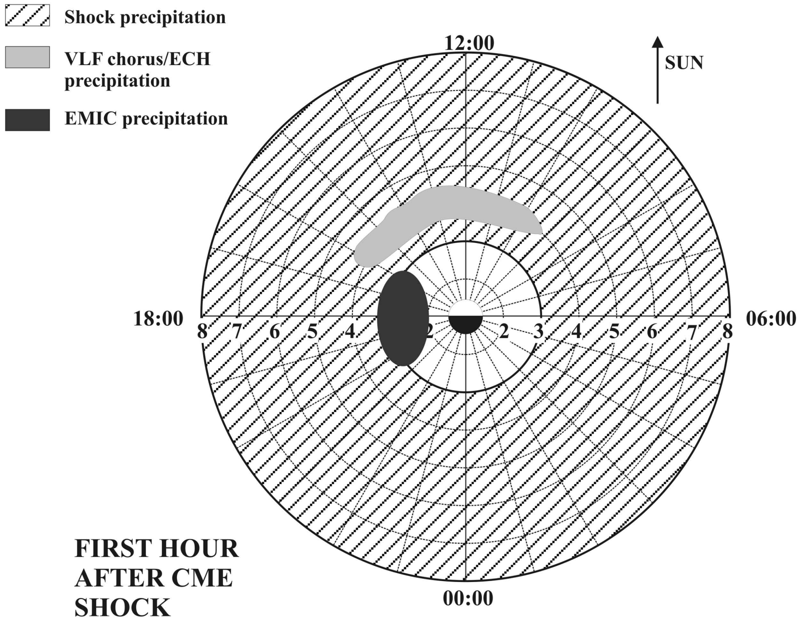
Shock precipitation
VLF chorus/ECH precipitation
EMIC precipitation
12:00
SUN
18:00
06:00
00:00
8 7 6 5 4 2 2 3 4 5 6 7 8
FIRST HOUR AFTER CME SHOCK